

# First Principle Thousand Atom Quantum Dot Calculations

Lin-Wang Wang and Jingbo Li

*Computational Research Division, Lawrence Berkeley National Laboratory, Berkeley, CA 94720*

(Dated: February 10, 2004)

A charge patching method and an idealized surface passivation are used to calculate the single electronic states of IV-IV, III-V, II-VI semiconductor quantum dots up to a thousand atoms. This approach scales linearly and has a 1000 fold speed-up compared to direct first principle methods with a cost of eigen energy error of about 20 meV. The calculated quantum dot band gaps are parametrized for future references.

PACS numbers: 71.15.-m, 73.21.La, 78.67.Hc

One major challenge in nanoscience is to calculate the nanosystems using first principle methods. Most nanosystems contain from a few thousands to a million atoms. Recently near thousand atom Si quantum dots have been calculated under the local density approximation (LDA) of the density functional theory using a real space grid on a massively parallel computer [1]. However, for many other materials and systems such calculations are still too laborious to be practical, especially because the standard LDA first principle calculations scale as  $O(N^3)$  of the system size  $N$ .  $O(N)$  methods have been studied for a decade, but it is still a research topic to this day [2]. Because of these difficulties, most current thousand atom electronic structure calculations are carried out using either the empirical tight-binding (TB) method or empirical pseudopotential method (EPM) based on some time unstable and often time consuming fitting procedures.

Another common problem for colloidal quantum dot simulation is the surface passivation. The experimental surface passivation of such systems are complicated. Large organic molecules are often used to passivate the quantum dot surface with the atomic details poorly understood [3]. These uncertainties and complexities have hindered the use of first principle methods to study the colloidal nanosystems. As a result, most first principle studies have been focused on Si quantum dots.

Here, we present a comprehensive approach which solves the above two problems simultaneously. This approach calculates the near-the-band-gap single electron states pertaining to the optical and transport properties of thousand atom colloidal nanosystems. While it gives essentially the same results as a traditional selfconsistent first principle LDA calculation, it could be a thousand times faster and it scales linearly to the size of the system.

The surface of an unpassivated nanocrystal consists of dangling bonds. An ideal passivation can be defined as making these dangling bonds re-bonded, and keeping the system locally charge neutral. If a surface atom has  $m$  valence electron, this atom provides  $m/4$  electrons to each of its four bonds in a tetrahedral crystal. To pair the  $m/4$  electron in each dangling bond, a passivating agent needs to provide  $(8-m)/4$  additional electrons. To keep the system locally neutral, there must be a posi-

tive  $(8-m)/4$  nuclear charge nearby from the passivating agent. Thus, the simplest ideal passivation agent will be a hydrogen-like atom with  $(8-m)/4$  electrons and a nuclear charge  $Z=(8-m)/4$ . This is the case for hydrogen passivated Si surfaces where  $Z=1$ . For III-V and II-VI systems,  $Z$  is not an integer, so the corresponding hydrogen-like atom will be a pseudo-atom (to be denoted as  $H'$ ). But this pseudo-atom does capture the essential characteristics of any real good passivation agents, thus can serve as an simplified approximation of those real passivation agents.

We will use the hydrogen-like pseudo atoms  $H'$  as approximated ideal passivation agents for all the real passivations. In the real world, when the experimental surface passivation is getting better, their results will approach this  $H'$  passivation results. Note that, this hydrogen-like pseudo atom has been widely used in thin film calculations [4] to passivate the unwanted back surface atoms. Here, we have elevated it to a physical model as the limit of ideal passivations. We have used  $Z=1, 0.75, 0.5, 1.25, 1.5$  for IV, V, VI, III, II row atoms respectively. A half bulk bond length is used as the  $H'$  atom - surface atom bond length for all the systems. We have studied Si, GaAs, InP, InAs, CdSe, CdTe, CdS semiconductors. All the occupied  $H'$ -surface atom bonds are deep inside the valence band and there is no remaining band gap states. For these good passivations, the band edge states do not depend on the passivation details. We have used planewave norm conserving pseudopotentials for all the above systems with an planewave energy cutoff of 25 Ryd (except for CdSe where 35 Ryd is used).

To solve the computational problem of the large sizes of the quantum dots, we have used the charge patching method [5, 6]. This method has been used for isoelectronic impurity states, alloys and carbon fullerenes, but it has never been used for a system with a surface, nor it has been used for surface passivations. Its applicability to colloidal systems was not known. In a charge patching method, it is assumed that the charge density at a given point depends only on the local atomic environment around that point. As a result, charge density motifs for all the atoms can be calculated from prototype systems, and can then be used to reassemble the charge density of a large system. A charge density motif is calculated as:

$$m_{I_\alpha}(\mathbf{r} - \mathbf{R}_\alpha) = \rho_{LDA}(\mathbf{r}) \frac{w_\alpha(|\mathbf{r} - \mathbf{R}_\alpha|)}{\sum_{\mathbf{R}_{\alpha'}} w_{\alpha'}(|\mathbf{r} - \mathbf{R}_{\alpha'}|)} \quad (1)$$

here  $\mathbf{R}_\alpha$  is a atomic site of atom typed  $\alpha$ , and  $m_{I_\alpha}(\mathbf{r} - \mathbf{R}_\alpha)$  is the charge density motif belonging to this atomic site, and  $\rho_{LDA}(\mathbf{r})$  is the selfconsistently calculated charge density of a prototype system. We have used the atomic charge density of the atom  $\alpha$  multiplied by an exponential decay function as  $w_\alpha(r)$  in Eq(1). The calculated localized  $m_{I_\alpha}(\mathbf{r} - \mathbf{R}_\alpha)$  is stored in a numerical array. We have used a subscript  $I_\alpha$  in  $m_{I_\alpha}$  to denote the atomic bonding environment of the atom  $\alpha$  at  $\mathbf{R}_\alpha$ . This atomic bonding environment can be defined as the nearest neighbors atomic types of atom  $\alpha$ .

To reconstruct the charge density of a given system, the charge motifs for all the atoms are placed together:

$$\rho_{patch}(\mathbf{r}) = \sum_{\mathbf{R}_\alpha} m_{I_\alpha}(\mathbf{r} - \mathbf{R}_\alpha) \quad (2)$$

here the atomic bonding environment  $I_\alpha$  should be the same as in Eq(1).

After  $\rho_{patch}(\mathbf{r})$  is obtained, LDA formula can be used to generate the total potential and the Hamiltonian of a given system. Then, the linear scaling folded spectrum method (FSM) [7] can be used to solve the LDA band edge states for a thousand atom system. Note that, our current method is based on the LDA calculation, it is thus affected by the LDA band gap error. But as shown recently by Delerue *et. al.* [8], the difference between the GW quasiparticle energy and the LDA eigen energy in a nanosystem comes mainly from a macroscopic surface polarization term (besides the constant bulk differences). As a result, the GW energies can be obtained from the LDA Kohn-Sham eigen energies following a simple procedure [8]. In the following, however, we will constrain ourselves to the LDA band edge states.

A bulk unit cell, a (111) thin film and a (001) thin film are used as our prototype systems. From these three prototype systems, using Eq(1), we can get the charge motifs for cation and anion with 0, 1, and 2 'H' bonds (we have removed any surface atom with 3 'H' bonds). At the same time, we can also get the charge motifs for the 'H' atoms. All these systems contain about 10 atoms. Thus the whole pre-calculations to generate the motifs don't take much time and the whole procedure can be automatized.

The accuracy of the patched charge density  $\rho_{patch}(\mathbf{r})$  of Eq(2) can be measured by its difference to the directly calculated selfconsistent LDA charge density  $\rho_{LDA}(\mathbf{r})$ :  $\Delta\rho = \int |\rho_{patch}(\mathbf{r}) - \rho_{LDA}(\mathbf{r})| d^3\mathbf{r} / \int \rho_{LDA}(\mathbf{r}) d^3\mathbf{r}$  and the eigen energy differences between the charge patching results and the direct LDA results. These are shown in Table.I for different systems. Notice that, for the bulk system, the error is only caused by numerical interpolations. The  $Cd_{79}Se_{68}$ ,  $Ga_{79}As_{68}$  and  $Si_{147}$  are spherical

quantum dots. Overall, we get a charge density error less than 1%, and an eigen energy error around 20 meV, similar to what we get for semiconductor alloys and carbon fullerenes [6]. Mind that, these errors are similar to the errors of the ab initio calculation introduced by different pseudopotentials and planewave basis sets. Thus, we can claim that the charge patching method is within the accuracy of the first principle calculations.

For all the AB (A: cation atom; B: anion atom) zinc blende semiconductor materials considered here, we have calculated:  $A_{79}B_{68}$ ,  $A_{141}B_{152}$ ,  $A_{321}B_{312}$ ,  $A_{495}B_{484}$ , and  $A_{675}B_{652}$  quantum dots. We found the charge densities of both the conduction band minimum (CBM) and valence band maximum (VBM) states are well inside the quantum dots for all the cases, indicating well surface passivation. Under the current procedure, it takes about one hour on 64 IBM SP processors to calculate one state for the largest quantum dot (e.g.,  $In_{675}P_{652}$ ). If the traditional  $O(N^3)$  direct LDA method were used, such calculation would take more than a month on the same computer. The speed up is more than 1000 times.

In Figures 1 and 2, the CBM, VBM eigen energy shifts and band gaps as functions of the quantum dot radius are shown for CdSe and Si quantum dots respectively. The eigen energies are aligned by the potentials inside the quantum dots. From Fig.1, we see that for CdSe, the quantum confinements for the CBM are much larger than the quantum confinements for the VBM. This is typical for all the direct band gap material because the effective mass of the electron is typically smaller than the hole. However, for Si, the situation is the opposite due to the indirect nature of its band gap. The Si effective mass for the electron near the X point is larger than the hole effective masses. The small CBM confinement compared to VBM is in agreement with the experimental result [9].

In Fig.1(c), we have fitted the band gap confinement  $\Delta E_g$  as a function  $\beta/d^\alpha$  where  $d$  is the diameter of the quantum dot. The agreement is excellent. We find the same for all other calculated systems. The resulting  $\alpha$  and  $\beta$  are listed in Table.II for future references. They can also be used to extend the traditionally calculated LDA results [10] to much larger systems. We can see in Table.II that,  $\alpha$  is around 1.2 for all the II-VI systems, 1.0 for all the III-V systems, and 1.6 for the IV-IV Si. All these are far from the  $1/d^2$  simplistic effective mass scaling. Effective mass theory is based on the parabolic approximation of the band structure at the  $\Gamma$  point. For the quantum dot sizes considered here, the effective k-points could be at 30% of the Brillouin zone boundary, thus far beyond the parabolic approximation. Thus, although we have used effective masses as guides in our qualitative arguments above, the effective mass theory cannot be used as a quantitative theory to predict the results in the quantum dot size range studied here. The  $1/d^2$  effective mass scaling will only appear after  $d > 100\text{\AA}$  [11].

One interesting result we found is the conduction band of the GaAs quantum dot. In the bulk, the L and X

points of the GaAs is only 0.3 eV above the  $\Gamma$  point. As they have larger effective masses, under quantum confinement, they might become the bottom of the conduction band. For a Ga centered spherical quantum dot as we studied here, the different bulk valley points will fold into the quantum dot states as following:  $3X_{1c} \rightarrow t_2^{(3)}$ ;  $3X_{3c} \rightarrow e^{(2)} + a_1^{(1)}$ ;  $4L_{1c} \rightarrow t_2^{(3)} + a_1^{(1)}$ ;  $\Gamma_{1c} \rightarrow a_1^{(1)}$ , here the number in the bracket is the degree of degeneracy for that state. The same symmetry states (e.g.,  $a_1$  and  $t_2$ ) from different valleys will intermix. In Fig.3(a), we have shown two  $a_1$  states, and one  $t_2$  state [12]. For the two  $a_1$  states, we have used the size of the spherical symbol to represent the relative magnitude of the oscillator strength  $|\langle a_1 | P | VBM \rangle|^2$ , which is also a rough measurement of the  $\Gamma$  point component in  $a_1$ . We see that the first  $a_1$  state changes from a  $\Gamma$ -like state in large quantum dot to a L-like state in smaller dot, and the second  $a_1$  state behaves just the opposite. Thus around  $d = 2.7$  nm there is a  $\Gamma - L$  transition between these two  $a_1$  states. This is the first time such transitions are shown explicitly following the size change at ambient pressure. This is also different from previous EPM results [13].

Under the same procedure, we also calculated the GaAs quantum wire along the (111) direction as shown in Fig.3(b). Here, the  $L$  point will not fold into the  $\bar{\Gamma}$  of the wire. What relevant is the X point. The X point folded state and the  $\Gamma$  point state anticross at  $d=2.5$  nm.

The transitions shown here can be detected from the intensity change of the photoluminescence, and the study of such transitions will reveal the electronic structure of the system.

To demonstrate the versatility of the current approach, we have shown in Fig.4 a thousand atom wurtzite CdTe/CdSe quantum rod (half of the rod is CdTe and the other half is CdSe) with H<sup>+</sup> surface passivations. The atomic positions are relaxed by valence force field method which describes the elastic aspects of the system accurately [5, 6]. In order to deal with the relaxed atomic positions, motif derivatives in regard to the bond length and angle changes have been used as described in Ref.[6]. Figure 4 shows that the CBM is localized mostly at the CdSe side while the VBM is localized most at the CdTe side. This gives us an approach to manipulate the electronic structures and transport properties of such nanosystems. Due to the existence of many competing factors (e.g., band alignment, strain effect, different effective masses), reliable first principle accuracy calculations like this is critical to determine the electronic properties of such systems, hence to realize materials by design.

This work was supported by U.S. Department of Energy under Contract No. DE-AC03-76SF00098. This research used the resources of the National Energy Research Scientific Computing Center.

- 
- [1] J. R. Chelikowsky, J. Phys. D **33**, R33 (2000).  
 [2] J.-L. Fattebert and J. Bernholc, Phys. Rev. B **62**, 1713 (2000).  
 [3] A. P. Alivisatos, J. Phys. Chem. **100**, 13226 (1996).  
 [4] K. Shiraishi, J. Phys. Soc. Jap. **59**, 3455 (1990).  
 [5] L.W. Wang, App. Phys. Lett. **78**, 1565 (2001).  
 [6] L.W. Wang, Phys. Rev. B **65** 153410 (2002); L.W. Wang, Phys. Rev. Lett. **88**, 256402 (2002).  
 [7] L.W. Wang and A. Zunger, J. Chem. Phys. **100**, 2394 (1994).  
 [8] C. Delerue, G. Allan, M. Lannoo, Phys. Rev. Lett. **90**, 76803 (2003).  
 [9] T. van Buuren, T. Tiedje, J.R. Dahn and B.M. Way, Appl. Phys. Lett. **63**, 2911 (1993).  
 [10] See for example: L.G. Wang, S.J. Pennycook, and S.T. Pentelides, Phys. Rev. Lett. **89**, 75506 (2002).  
 [11] Y. M. Niquet, C. Delerue, G. Allan, and M. Lannoo, Phys. Rev. B **62**, 5109 (2000); Appl. Phys. Lett. **77**, 1182 (2000).  
 [12] To calculate Fig.3, we have slightly adjusted the Ga and As nonlocal pseudopotentials, so the resulting electron effective mass,  $E(X_{1c} - \Gamma)$ , and  $E(L_{1c} - \Gamma)$  are 0.067 m, 0.496 eV, and 0.288 eV respectively, agreeing well with the corresponding experimental values of 0.066 m, 0.46 eV, and 0.29 eV.  
 [13] A. Franceschetti and A. Zunger, Appl. Phys. Lett. **68**, 3455 (1996).

system	$\Delta\rho$	$\Delta E_g$ (meV)
bulk_CdSe	0.01%	$2 \times 10^{-4}$
(100)_CdSe	0.40%	30
(111)_CdSe	0.47%	32
(110)_CdSe	0.46%	17
(110)_GaAs	0.55%	0.5
(110)_Si	0.54%	9
Cd <sub>79</sub> Se <sub>68</sub>	0.79%	11
Ga <sub>79</sub> As <sub>68</sub>	0.71%	9
Si <sub>147</sub>	0.67%	7

TABLE I: The accuracy of the charge patching method compared to direct self-consistent LDA calculations. The eigen energy errors for all other eigenstates are similar to the band gap errors shown here. The eigen state energy splittings in the quantum dot has a typically error of a few meV. E.g., for the Si<sub>146</sub> quantum dot, the LDA calculated splitting energies for CBM3-CBM2, CBM2-CBM1, VBM1-VBM2, VBM2-VBM3 are 18, 7, 113, and 7 meV respectively, while the charge patching results are 16, 8, 118, and 9 meV. For the same dot, after a spectrum alignment, the maximum error in all the valence band energies is 14 meV, while the averaged error is 6 meV.

	Si	GaAs	InAs	InP	CdSe	CdS	CdTe
$\beta$	3.81	3.88	4.41	3.90	3.84	3.35	4.40
$\alpha$	1.60	1.01	1.01	1.10	1.18	1.22	1.28

TABLE II: The  $\alpha$  and  $\beta$  for the  $\beta/d^\alpha$  fit of the  $\Delta E_g$  for different materials. The unit of  $\beta$  is eV $\times$ Bohr $^\alpha$ .

FIG. 1: The CBM and VBM band energy shifts from the bulk values (a), and the change of band gap  $\Delta E_g$  (b) as functions of the diameter  $d$  of the spherical CdSe quantum dot. (c) is a fit of  $\Delta E_g$  as  $\beta/d^\alpha$ .

FIG. 2: The same as Fig.2, except for Si quantum dots.

FIG. 3: (a) The  $a_1$  and  $t_2$  states in GaAs quantum dot, and (b) the  $\Gamma$ -like and X-like state anticrossing in (111) GaAs quantum wire. The diameter of the dark sphere in (a) is proportional to  $| \langle a_1 | P | VBM \rangle |^{2/3}$ .

FIG. 4: The isosurface plots of the wavefunction squares of CBM (a) and VBM (b) states for a CdTe/CdSe quantum rod. The total length of the rod is 10.6 nm and the diameter is 2 nm. The small dots are atoms.

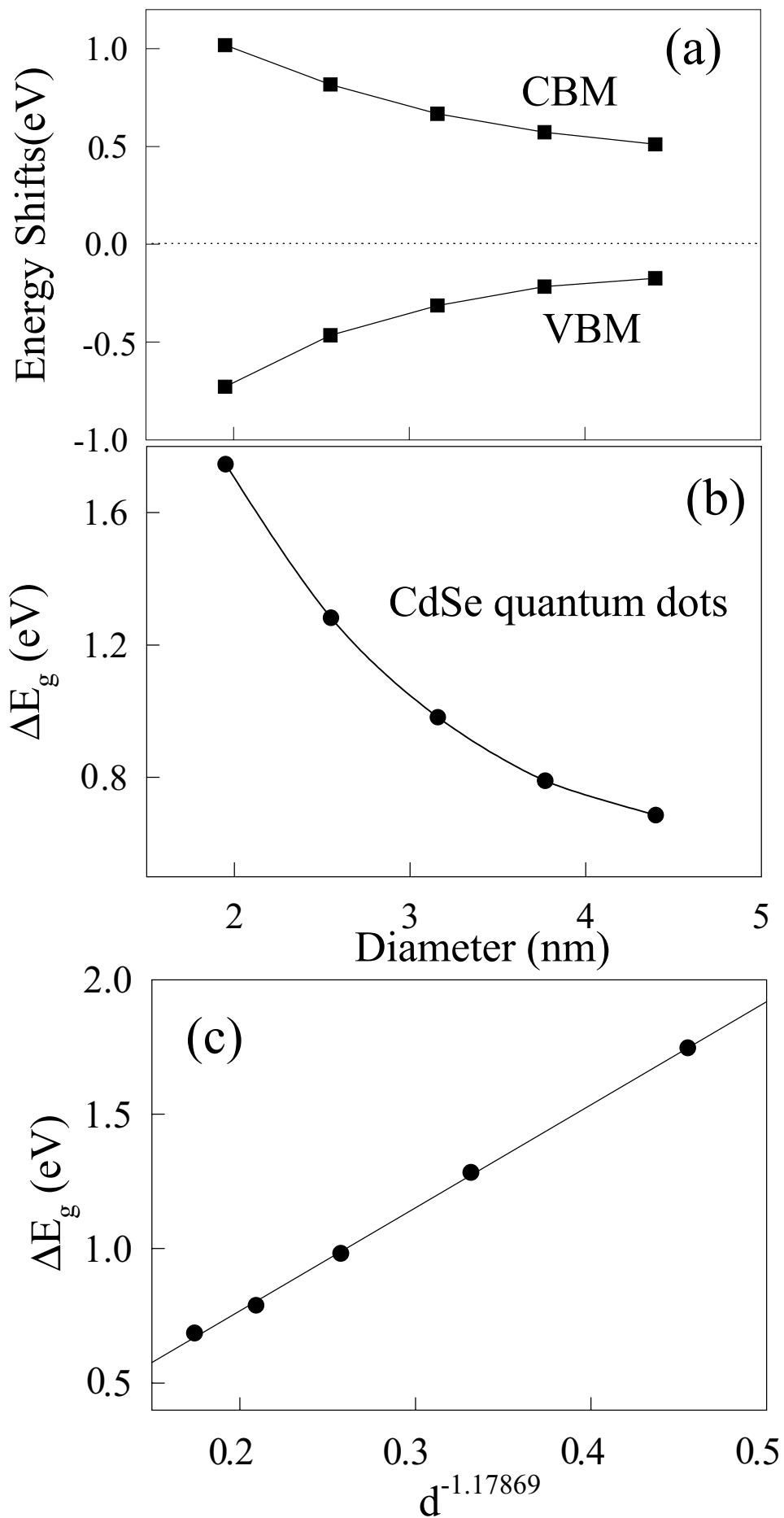


Fig. 1 Wang and Li

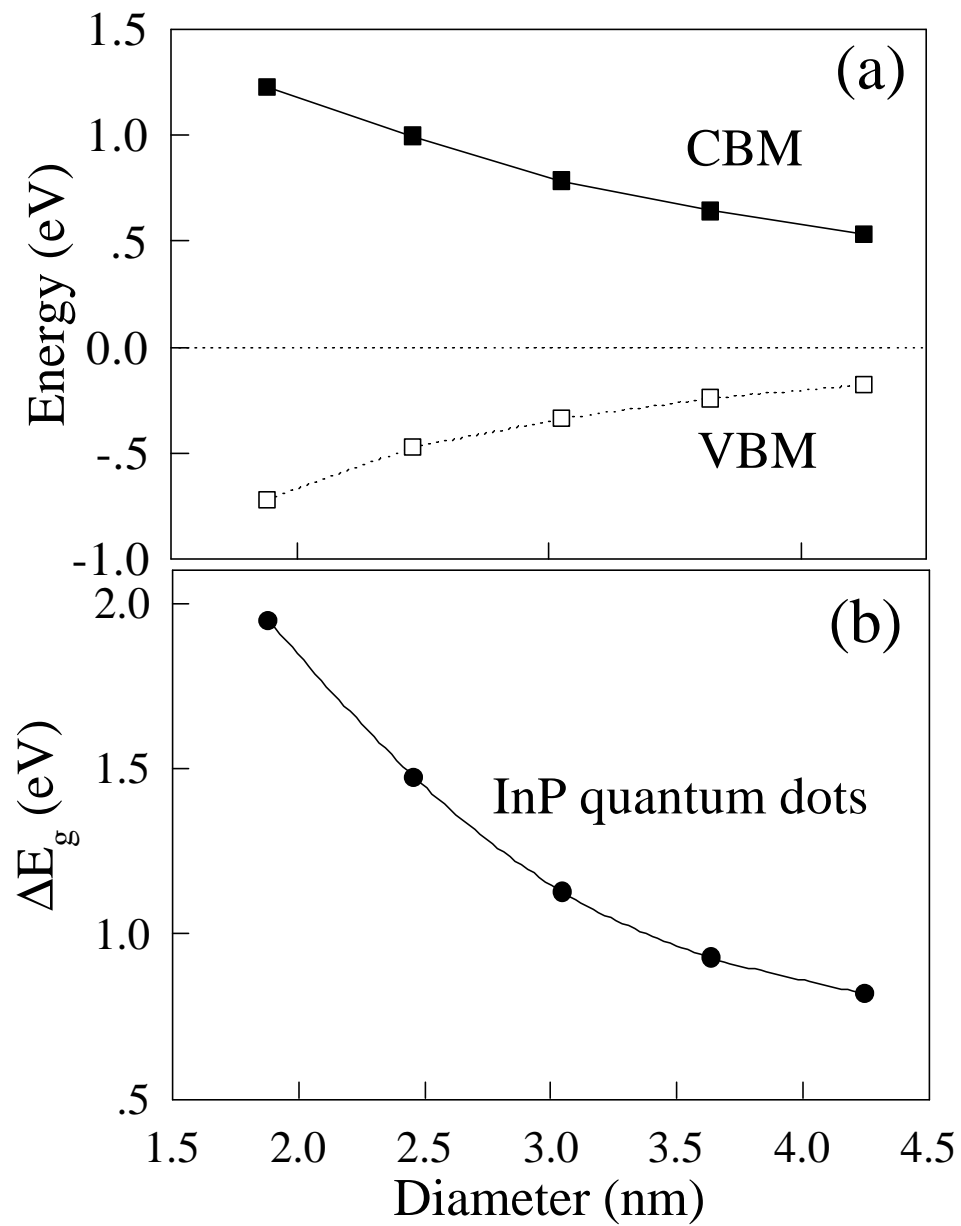


Fig. 3 Wang and Li

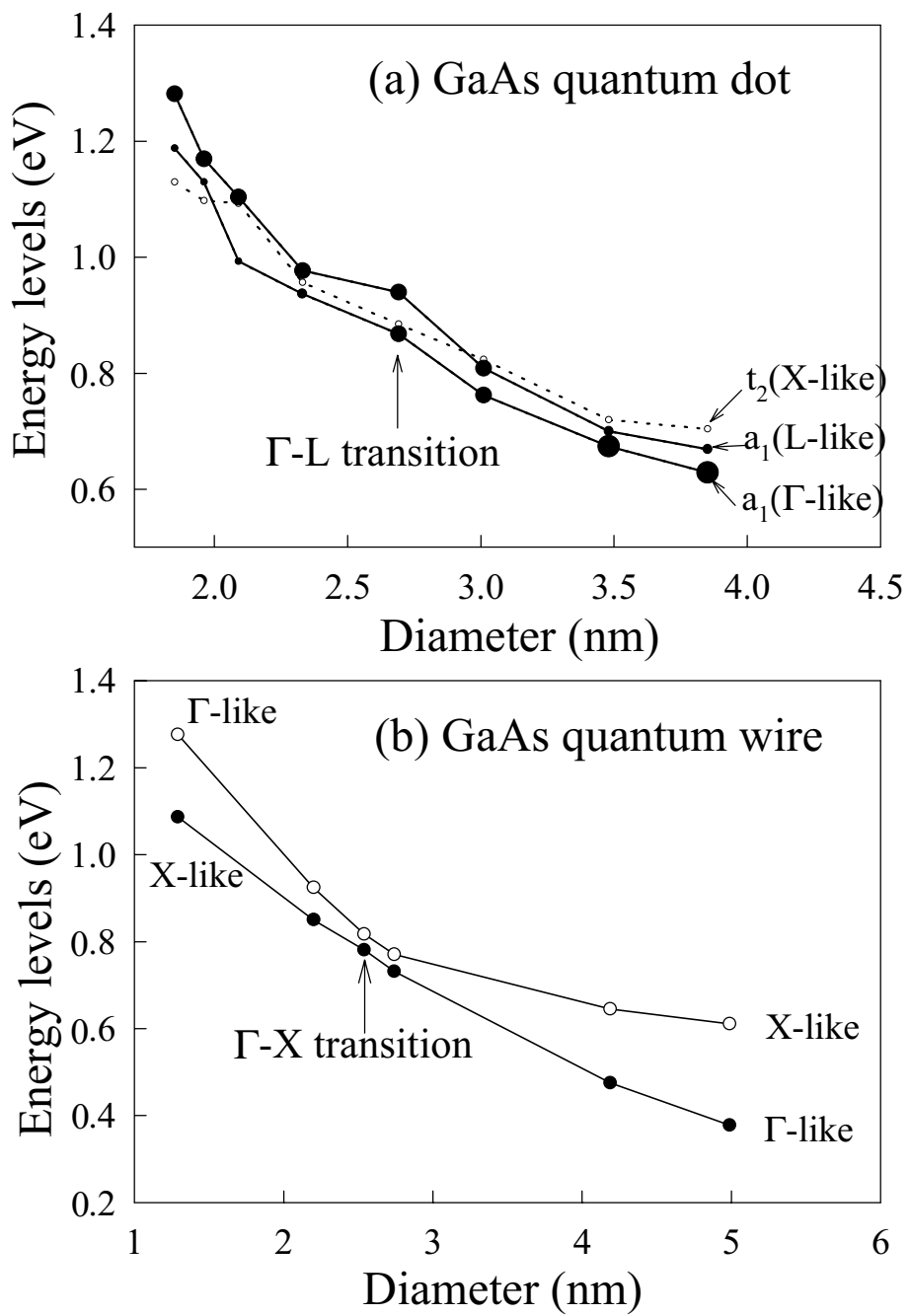


Fig. 3 Wang and Li

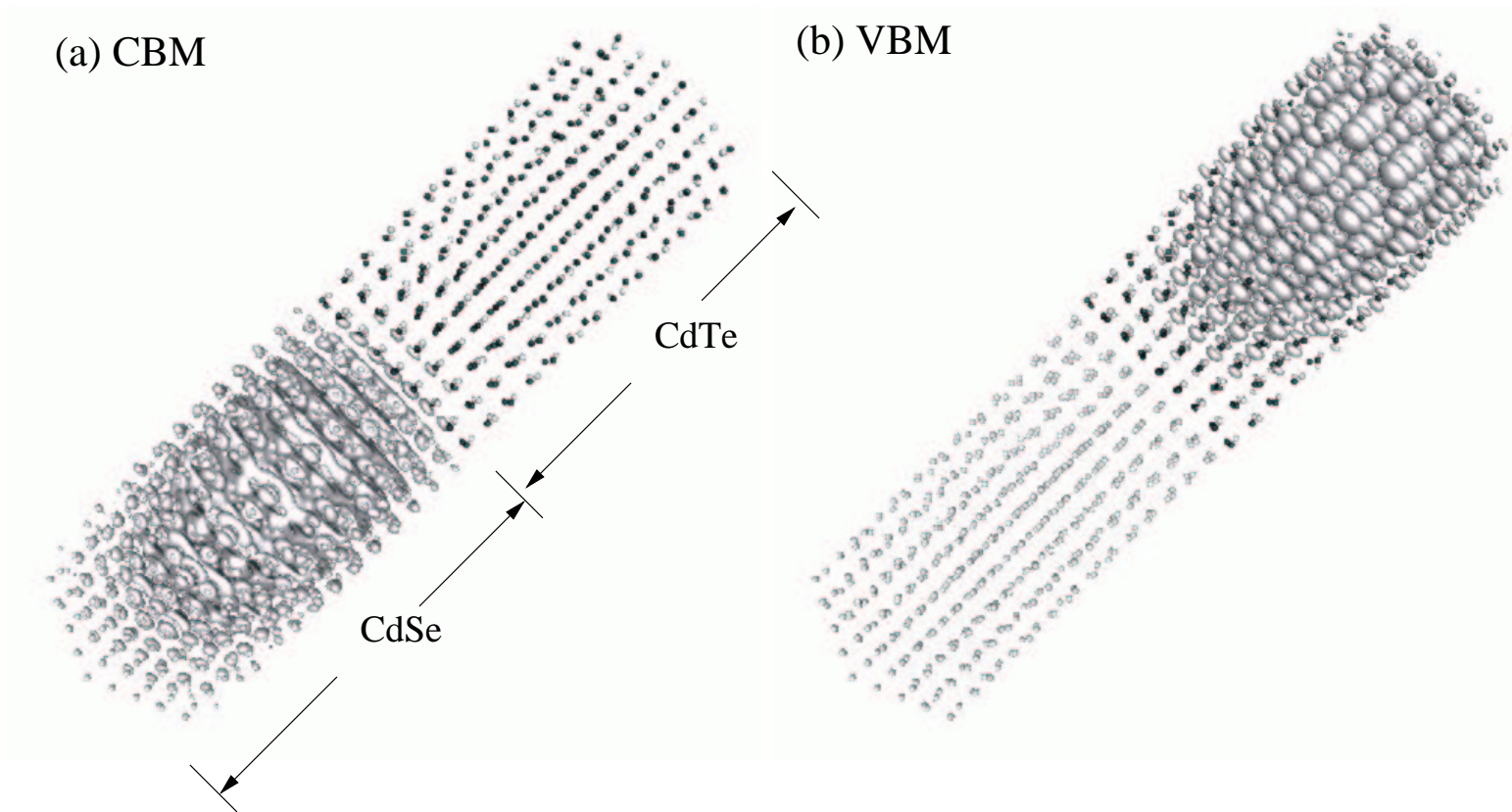


Fig. 4 Wang and Li